

# Effect of bismuth doping on the physical properties of La–Li–Mn–O manganite

Kalyana Lakshmi Yanapu<sup>1,4</sup> · S. Shanmukharao Samatham<sup>2</sup> · Devendra Kumar<sup>3</sup> · V. Ganesan<sup>2</sup> · P. Venugopal Reddy<sup>4</sup>

Received: 5 June 2015 / Accepted: 2 October 2015 / Published online: 25 February 2016  
© Springer-Verlag Berlin Heidelberg 2016

**Abstract** The effects of bismuth doping at La site on magnetic, electrical and thermopower properties of LaLiMnO<sub>3</sub> manganites have been investigated. The substitution of Bi ion leads to the weakening of ferromagnetic ordering at low temperature, and Curie temperature ( $T_C$ ) decreases with increase in Bi content. Interestingly, a dramatic increase in the magnitude of Seebeck coefficient at low temperature is observed in Bi-doped samples which might find potential application as thermoelectric. The results are attributed to the combined effect of the disorder and antiferromagnetic interaction induced by Bi doping. Both  $\rho(T)$  and  $S(T)$  data in the high-temperature region are discussed using small polaron hopping model.

## 1 Introduction

Observation of colossal magnetoresistive (CMR) effect [1–4] and half-metallic nature of the carriers at the Fermi level makes the perovskite manganites having general formula Ln<sub>1-x</sub>A<sub>x</sub>MnO<sub>3</sub> (Ln = rare earth ions; A = alkaline metals) materials of great scientific interest and ideal candidates for

spintronic applications. The properties of these materials are influenced by the parameters such as average sizes of the Ln site cations [5–7], the mismatch effect [8], the vacancy in Ln and Mn sites [9] and the oxygen stoichiometry [10, 11]. Thus, manganites are characterized by a complex interplay between structural, magnetic and electrical properties leading to rich phase diagram. The phase diagram of some of the divalent manganites shows that the compounds with  $0.2 < x < 0.5$  are ferromagnetic and metallic, whereas those with  $0.5 < x < 0.9$  are antiferromagnetic (AFM) and charge-ordered (CO). In a narrow region around  $x = 0.5$ , dissimilar ground states are thought to exist [12–14]. The simultaneous occurrence of ferromagnetic (FM) and metallic states has been qualitatively explained by the double-exchange (DE) mechanisms [15] combining with the local Jahn–Teller (JT) distortions of Mn<sup>3+</sup> ions [16]. In addition to divalent doping, perovskite manganites doped with monovalent alkali-metal ions have been studied and still interest the scientific community [17–20]. Due to the difference in the valence, alkaline-earth-metal and alkali-metal doping in LaMnO<sub>3</sub> can result in remarkably different consequences. Among the various monovalent-doped manganites, lithium ion substituted one is interesting due to CMR over a wide temperature range [17, 18]. According to the calculation of tolerance factor, LaLiMnO<sub>3</sub> system forms a stable manganite resulting in interesting electrical and magnetic properties.

Over the past few years, extensive work has been carried out on the partial substitution of the A-site using trivalent or divalent ion [21–23] and the changes in the electrical properties were discussed based on structural effects. Unlike lanthanide ions, substitution of a non-magnetic ion such as bismuth (Bi) at A-site shows strong effects on electrical and magnetic properties of manganites because it

✉ Kalyana Lakshmi Yanapu  
kalyanalakshmiyanapu@gmail.com

<sup>1</sup> Department of Physics, Nizam College, Osmania University, Hyderabad, Telangana, India  
<sup>2</sup> Low Temperature Laboratory, UGC-DAE Consortium for Scientific Research, University Campus, Khandwa Road, Indore 452001, M.P., India  
<sup>3</sup> UGC-DAE Consortium for Scientific Research, University Campus, Khandwa Road, Indore 452001, M.P., India  
<sup>4</sup> Department of Physics, University College of Science, Osmania University, Hyderabad, Telangana, India

is stable with an oxidation state 3+ and has an average ionic radius consistent with the geometrical rule of the tolerance factor. Recently, several authors have reported electrical and magnetic properties of Bi doping in  $\text{La}_{0.67}\text{Ca}_{0.33}\text{MnO}_3$  [24, 25] and  $\text{La}_{0.5}\text{Ca}_{0.5}\text{MnO}_3$  [26] compounds. These studies have indicated that magnetoresistance (MR) increases with Bi doping. To the best of our knowledge, there are no reports on the Bi-doped  $\text{LaLiMnO}_3$  manganites. Since the ionic radii of trivalent bismuth and trivalent lanthanum are very close to each other, one may expect similar electrical transport and magnetic properties between them. Therefore, it would be interesting to study the magnetotransport properties of these materials by substituting bismuth at Ln site. For this, the samples having compositions  $\text{La}_{5/6-x}\text{Bi}_x\text{Li}_{1/6}\text{MnO}_3$  with  $x = 1/6$  and  $\text{La}_{3/4-x}\text{Bi}_x\text{Li}_{1/4}\text{MnO}_3$  with  $x = 1/4$  (a conservation of charge balance requires that two ions of  $\text{Mn}^{3+}$  transforms into the state of  $\text{Mn}^{4+}$  per each monovalent ion substitution) are chosen by keeping their  $\text{Mn}^{3+}/\text{Mn}^{4+}$  constant, and their results were compared with the undoped ones. In view of the above facts, an effort has been made to study the structural, magnetic and transport properties of Bi doping in  $\text{LaLiMnO}_3$  manganite.

## 2 Experimental details

Four samples of compositions  $\text{La}_{5/6}\text{Li}_{1/6}\text{MnO}_3$ ,  $\text{La}_{2/3}\text{Bi}_{1/6}\text{Li}_{1/6}\text{MnO}_3$ ,  $\text{La}_{3/4}\text{Li}_{1/4}\text{MnO}_3$  and  $\text{La}_{1/2}\text{Bi}_{1/4}\text{Li}_{1/4}\text{MnO}_3$  were synthesized by a wet chemical method using polyvinyl alcohol (PVA),  $\text{La}_2\text{O}_3$ ,  $\text{LiCO}_3$ ,  $\text{Bi}(\text{NO}_3)_3 \cdot 5\text{H}_2\text{O}$ , and manganese acetate. Prescribed ratios of starting materials were dissolved in nitric acid and distilled water to make a clear solution. An aqueous polymer solution of PVA and sucrose were added to the stock solution, and the above mixture was stirred to promote the dissolution and reaction. After the mixture became transparent solution, it was dried slowly on a hot plate until gel was formed and then heated to give a brown powder. This precursor was calcined and pressed into circular pellets and sintered at 1223 K for 2 h. The phase purity, homogeneity and cell dimensions were determined by powder X-ray diffraction (XRD) at room temperature. Structural refinement was carried out using the standard Rietveld refined technique. The estimation of cations in the sample was carried out by inductively coupled plasma-atomic emission spectroscopy (ICP-AES, JY 2000), while the valence state of Mn was determined by iodometric redox titration method. Magnetization measurements were performed on a vibrating sample magnetometer (MPMS, QD-USA). The transport and magnetotransport measurements were carried out using four-probe method (14 T/2.0 K PPMS, QD-USA) in an applied magnetic field strengths of 10, 50, 100 kOe over a

temperature range 10–400 K. Finally, the thermoelectric power (TEP) measurements were carried out on an automated precision measurement system [27]. For the ease of notation, the samples with compositions  $\text{La}_{5/6}\text{Li}_{1/6}\text{MnO}_3$ ,  $\text{La}_{2/3}\text{Bi}_{1/6}\text{Li}_{1/6}\text{MnO}_3$ ,  $\text{La}_{3/4}\text{Li}_{1/4}\text{MnO}_3$  and  $\text{La}_{1/2}\text{Bi}_{1/4}\text{Li}_{1/4}\text{MnO}_3$  are referred using the notation LLP 33, LLB 33, LLP 50 and LLB 50.

## 3 Results and discussion

### 3.1 Structural

The room-temperature XRD patterns of the samples of the present investigation are shown in Fig. 1 and found that the samples are single phase with no detectable secondary phase. The collected patterns were indexed based on rhombohedral symmetry with R-3c space group. The structural parameters of the samples were refined by the

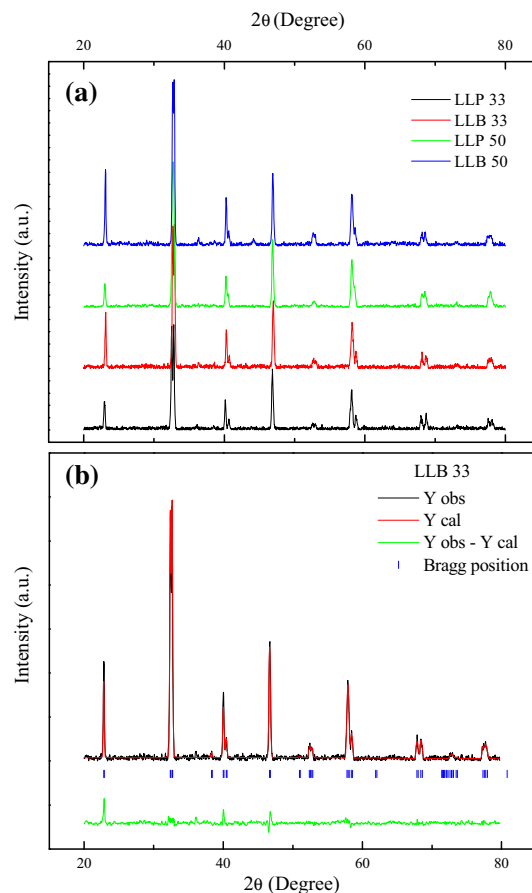


**Fig. 1** **a** Room-temperature powder X-ray diffraction patterns of  $\text{La}_{5/6}\text{Li}_{1/6}\text{MnO}_3$ ,  $\text{La}_{2/3}\text{Bi}_{1/6}\text{Li}_{1/6}\text{MnO}_3$ ,  $\text{La}_{3/4}\text{Li}_{1/4}\text{MnO}_3$  and  $\text{La}_{1/2}\text{Bi}_{1/4}\text{Li}_{1/4}\text{MnO}_3$  samples from 20° to 80°. **b** Rietveld refined pattern of  $\text{La}_{2/3}\text{Bi}_{1/6}\text{Li}_{1/6}\text{MnO}_3$  manganite with standard peak positions (blue vertical lines) and fit (solid line) of the model to the intensities. The green solid line at the bottom is the difference spectrum

**Table 1** Rietveld refined parameters of undoped and doped (Bi) LLMO manganite

| Sample composition           | La <sub>5/6</sub> Li <sub>1/6</sub> MnO <sub>3</sub> | La <sub>2/3</sub> (Li <sub>1/6</sub> Bi <sub>1/6</sub> )MnO <sub>3</sub> | La <sub>3/4</sub> Li <sub>1/4</sub> MnO <sub>3</sub> | La <sub>1/2</sub> (Li <sub>1/4</sub> Bi <sub>1/4</sub> )MnO <sub>3</sub> |
|------------------------------|------------------------------------------------------|--------------------------------------------------------------------------|------------------------------------------------------|--------------------------------------------------------------------------|
| Sample code                  | LLP 33                                               | LLB 33                                                                   | LLP 50                                               | LLB 50                                                                   |
| <i>a</i> (Å)                 | 5.513                                                | 5.522                                                                    | 5.502                                                | 5.532                                                                    |
| <i>b</i> (Å)                 | 5.513                                                | 5.522                                                                    | 5.502                                                | 5.532                                                                    |
| <i>c</i> (Å)                 | 13.324                                               | 13.375                                                                   | 13.392                                               | 13.402                                                                   |
| Volume (Å <sup>3</sup> )     | 350.8                                                | 353.3                                                                    | 352.5                                                | 354.3                                                                    |
| $\langle r_A \rangle$ (Å)    | 1.120                                                | 1.121                                                                    | 1.100                                                | 1.102                                                                    |
| $\tau$                       | 0.8880                                               | 0.8885                                                                   | 0.8894                                               | 0.8903                                                                   |
| $\sigma^2$ (Å <sup>2</sup> ) | 0.0079                                               | 0.0081                                                                   | 0.0108                                               | 0.0111                                                                   |
| Mn–O–Mn (°)                  | 161.93                                               | 161.04                                                                   | 163.64                                               | 163.62                                                                   |
| Mn–O (Å)                     | 1.965                                                | 1.972                                                                    | 1.964                                                | 1.967                                                                    |
| Oxygen stoichiometry         | –                                                    | –                                                                        | –0.08                                                | –0.07                                                                    |

standard Rietveld technique, and the obtained parameters are given in Table 1. The ICP-AES analysis indicates that the average concentrations of La, Li, Bi and Mn are very close to the nominal composition within experimental errors, suggesting that samples used are of good quality. The values of Mn<sup>4+</sup>/Mn<sup>3+</sup> ratio and oxygen content determined by iodometric titrations are close to their nominal compositions in the case of LLP 33 and LLB 33, while the other two samples, i.e., LLP 50 and LLB 50, exhibit oxygen deficiency.

### 3.2 Magnetic studies

In order to study the evolution of the magnetic properties with Bi doping, the temperature dependence of magnetization  $M(T)$  measurements was performed in both zero-field-cooled (ZFC) and field-cooled (FC) modes under an applied magnetic field of 500 Oe and the results are shown in Fig. 2. It is clear from the figure that all the samples undergo paramagnetic (PM) to ferromagnetic (FM) transition ( $T_C$ ) with decreasing temperature. The values of  $T_C$  estimated from the minimum of the  $dM/dT$  against  $T$  plot are given in Table 2. It can be noticed from the results of the present investigation that doping of Bi at La site produces a significant change in the magnetic properties. The  $T_C$  and magnitude of magnetization at low temperature decrease with increasing Bi content, and this clearly indicates the weakening of ferromagnetic behavior in these samples. Similar results were reported in the case of Bi-doped divalent manganites [28]. It is well known that the A-site cationic size and Mn valency affect the ground state of the manganese compounds. Since the ionic radii of La<sup>3+</sup> are almost similar to those of Bi<sup>3+</sup> ion and that there is no change of the Mn valence in these compounds, the observed variation may be ascribed to the role of the 6s<sup>2</sup> lone-pair electrons of Bi ions [29]. Due to the competition

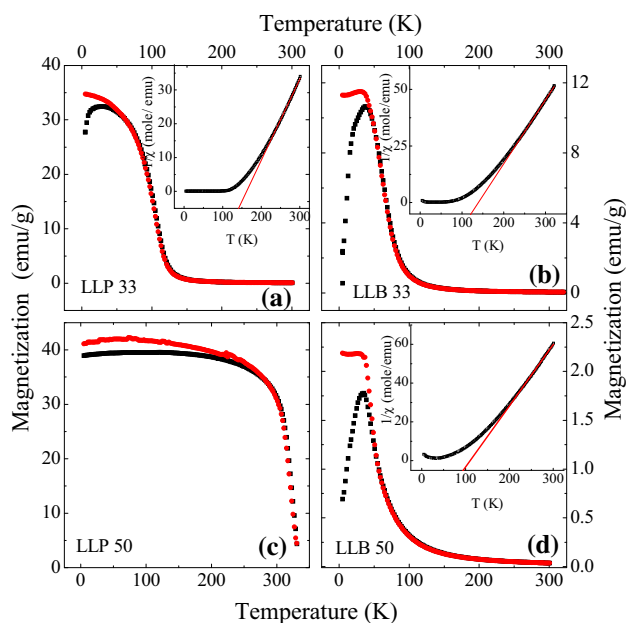


**Fig. 2** Temperature dependence of DC magnetization of La<sub>5/6</sub>Li<sub>1/6</sub>MnO<sub>3</sub>, La<sub>2/3</sub>Bi<sub>1/6</sub>Li<sub>1/6</sub>MnO<sub>3</sub>, La<sub>3/4</sub>Li<sub>1/4</sub>MnO<sub>3</sub> and La<sub>1/2</sub>Bi<sub>1/4</sub>Li<sub>1/4</sub>MnO<sub>3</sub> samples in ZFC (black squares) and FC (red circles) configurations. Inset shows the inverse susceptibility versus temperature curves of the samples, and the solid lines show the linear fitting at 500 Oe

between Bi<sup>3+</sup>: 6s<sup>2</sup> and Mn: t<sub>2g</sub> for the O: 2p electrons make the interaction (double exchange) between Mn<sup>3+</sup> and Mn<sup>4+</sup> weak leading to  $T_C$  shift toward low-temperature side [30]. Therefore, the reduction in  $T_C$  with bismuth substitution at La site may be explained based on the role of the 6s<sup>2</sup> lone-pair electrons of Bi ions. It can also be observed from Fig. 2 that there exists a bifurcation between the ZFC and FC curves below transition temperature and it is found to increase with increasing bismuth content. The bifurcation in ZFC–FC magnetization curves may occur due to

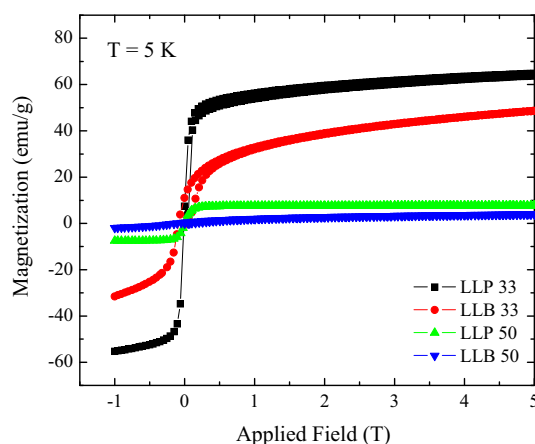
**Table 2** Experimental data and best fit parameters obtained from resistivity and thermopower data using SPH model

| Sample composition                | La <sub>5/6</sub> Li <sub>1/6</sub> MnO <sub>3</sub> | La <sub>2/3</sub> (Li <sub>1/6</sub> Bi <sub>1/6</sub> )MnO <sub>3</sub> | La <sub>3/4</sub> Li <sub>1/4</sub> MnO <sub>3</sub> | La <sub>1/2</sub> (Li <sub>1/4</sub> Bi <sub>1/4</sub> )MnO <sub>3</sub> |
|-----------------------------------|------------------------------------------------------|--------------------------------------------------------------------------|------------------------------------------------------|--------------------------------------------------------------------------|
| Sample code                       | LLP 33                                               | LLB 33                                                                   | LLP 50                                               | LLB 50                                                                   |
| $T_P$ (K)                         | –                                                    | –                                                                        | 283                                                  | –                                                                        |
| $T_C$ (K)                         | 105                                                  | 61                                                                       | >330                                                 | 45                                                                       |
| $\theta_{CW}$ (K)                 | 146                                                  | 125                                                                      | –                                                    | 95                                                                       |
| $\mu_{eff}$                       | 5.33                                                 | 5.28                                                                     | –                                                    | 5.02                                                                     |
| $\mu$ ( $\mu_B$ /Mn) at $H = 5$ T | 2.5                                                  | 2.0                                                                      | 2.9                                                  | 1.3                                                                      |
| $\alpha'$                         | –0.331                                               | –0.327                                                                   | –0.352                                               | –0.368                                                                   |
| $E_S$ (meV)                       | 157.4                                                | 170.7                                                                    | 170.7                                                | 183.4                                                                    |
| $E_P$ (meV)                       | 14.9                                                 | 21.8                                                                     | 24.1                                                 | 32.3                                                                     |

spin-glass, cluster-glass, superparamagnetic phase, coexistence of antiferromagnetic (AFM) and ferromagnetic (FM) phases, or even from an anisotropic ferromagnetic phase. A close observation of the magnetization results suggests the possibility of a spin-glass or cluster-glass-like state in Bi-doped samples.

In the paramagnetic state ( $T > T_C$ ), the magnetization curve is well fitted to the Curie–Weiss (CW) law, and the inset of Fig. 2 shows the  $T$  dependence of  $\chi^{-1}$  (susceptibility). The parameters obtained from the linear fit are given in Table 2. The CW temperature ( $\theta_{CW}$ ) is positive for all the samples, signaling predominantly FM exchange interaction in the samples. It can also be observed from the table that the effective magnetic moments ( $\mu_{eff}$ ) are considerably larger than the corresponding values calculated using the spin-only moments of manganese ions. These enhanced moments in the PM state can be ascribed to the appearance of magnetic clusters due to the short-range FM interaction [31].

In order to gain a deeper understanding of magnetic ground state with bismuth doping, the field-dependent magnetization measurements up to 50 kOe at  $T = 5$  K were carried out and the curves are shown in Fig. 3. In some samples, magnetization was measured up to 140 kOe (not shown). It can be noticed from the  $M(H)$  curves that the samples exhibit a small coercive field ( $H_C$ ) at low temperature which indicates soft ferromagnetic behavior. In the case of undoped samples (LLP 33 and LLP 50), magnetization values increase sharply in low magnetic field and remain almost constant with further increase in applied field. In contrast to this, there is a nonlinear increase of magnetization with increasing field and the sign of saturation is not observed even up to 140 kOe in case of Bi-doped samples. The unsaturated magnetization is the characteristic feature of AFM component in the system. The observed  $M(H)$  behavior in these samples might be due to the presence of different magnetic interactions. Therefore, at low temperatures there must be a subtle balance

**Fig. 3** Isothermal magnetization plots of La<sub>5/6</sub>Li<sub>1/6</sub>MnO<sub>3</sub>, La<sub>2/3</sub>Bi<sub>1/6</sub>Li<sub>1/6</sub>MnO<sub>3</sub>, La<sub>3/4</sub>Li<sub>1/4</sub>MnO<sub>3</sub> and La<sub>1/2</sub>Bi<sub>1/4</sub>Li<sub>1/4</sub>MnO<sub>3</sub> samples at  $T = 5$  K

between FM and AFM interactions; i.e., the system is phase-separated into FM and AFM clusters. Hence, there will always be a competition between these two interactions to dominate one over another giving rise to a tendency of glassy FM state in the sample [28]. Furthermore, the values of saturation magnetization ( $M_S$ ) were obtained from the high-field magnetization ( $H = 50$  kOe) and are given in Table 2. The  $M_S$  values estimated from the experimental data are found to be lower than the theoretical values. It has also been found that the obtained  $M_S$  values of bismuth-doped samples are smaller than the undoped ones and they also decrease with increase in Bi content. The disparity between the experimental and theoretical values also supports the coexistence of different interactions (FM and AFM) in these materials and with increasing bismuth content AFM interactions dominate over the FM interactions, thereby resulting in the reduction of  $M_S$  values. In fact, similar results were reported in the case of Bi-doped manganites [32].

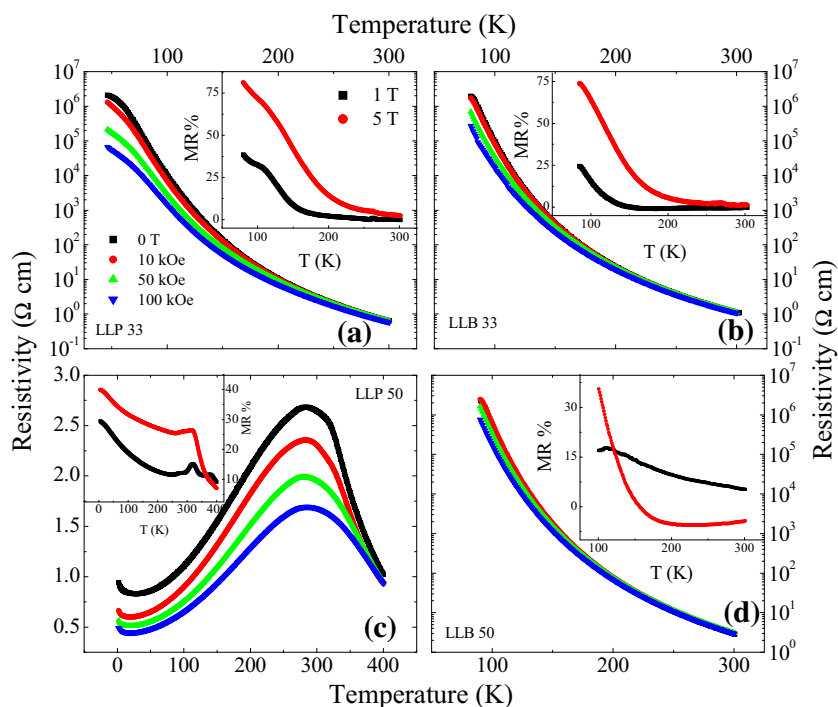
### 3.3 Transport studies

The variation of resistivity with temperature,  $\rho(T)$ , in LLP 33, LLB 33, LLP 50 and LLB 50 samples is shown in Fig. 4. It can be seen that except LLP 50 all the samples exhibit an insulating behavior over the measured temperature range (80–300 K). The resistivity values are very high at low temperature crossing instrumental limits. The observed results indicate the localization of charge carriers with Bi doping. It is well known that the magnetic and transport properties of perovskite manganites are sensitive to average A-site radius  $\langle r_A \rangle$ , oxygen stoichiometry, particle size, etc. As the ionic radii of  $\text{Bi}^{3+}$  are almost identical to  $\text{La}^{3+}$  ion,  $\langle r_A \rangle$  could not be the main factor in determining the properties of these materials. In fact, the variation in the electrical and magnetic behavior may be ascribed to the role of the  $6s^2$  lone-pair electrons of Bi ions [33]. Bi enhances the hybridization between  $6s^2$  orbitals of  $\text{Bi}^{3+}$  and  $2p$  orbitals of  $\text{O}^{2-}$  and produce a local distortion, and this in turn hinders the electron hopping between the Mn sites and leads to an effect on the electron transport to its neighbors [34]. Thus, the  $\text{Bi}^{3+}$ -doped samples exhibit insulating behavior. On the other hand, the high resistivity may also partially occur from the existence of grain boundaries [35].

The temperature dependence of resistivity for all the samples measured at applied magnetic fields of 10, 50 and 100 kOe is shown in Fig. 4. The insulating phase is robust even up to the external applied magnetic fields of 100 kOe in the case of LLP 33, LLB 33 and LLB 50 samples. In

fact, a similar behavior was reported in Bi-doped perovskites [30]. However, at low temperatures a decrease in resistivity is observed in the presence of magnetic field and the effect is weak in the case of LLB 50 sample. It is clear from the magnetization data that these samples show phase separation (competing FM and AFM interaction) in low-temperature region. In the compounds with competing magnetic orders, magnetic field favors one kind of order in the spins and results in magnetoresistance. In the samples of the present investigation, the charge transport is sensitive to the FM ordering and the magnetic field induces negative magnetoresistance below  $T_C$ . Hence, these samples show FM and insulating behavior with electronic phase separation in the low-temperature region. The plots of percentage of magnetoresistance (MR%) as a function of temperature are shown in the inset of Fig. 4. The MR% is calculated using the standard relation,  $\text{MR}\% = [\rho(0) - \rho(H)]/\rho(0)$ , where  $\rho(0)$  is the resistivity at zero field and  $\rho(H)$  is the resistivity at an applied magnetic field. It is clear from the figure that the LLP 50 sample shows two different kinds of MR behavior, one near  $T_P$  and the other in the low-temperature region. One of them is due to spin tunneling across the grain boundaries [36], and this contribution is more significant at low temperatures and low magnetic fields. The other contribution comes from the suppression of magnetic fluctuation as the field is increased and takes place within the volume of the grains and MR is dominant in the vicinity of the transition temperature. On the other hand, LLP 33, LLB 33 and LLB 50 compounds MR% increases with decreasing

**Fig. 4** Resistivity as a function of temperature for  $\text{La}_{5/6}\text{Li}_{1/6}\text{MnO}_3$ ,  $\text{La}_{2/3}\text{Bi}_{1/6}\text{Li}_{1/6}\text{MnO}_3$ ,  $\text{La}_{3/4}\text{Li}_{1/4}\text{MnO}_3$  and  $\text{La}_{1/2}\text{Bi}_{1/4}\text{Li}_{1/4}\text{MnO}_3$  samples at different magnetic field strengths ( $H = 0, 10, 50$  and  $100$  kOe). *Inset* of the figure represents the temperature dependence of percentage of magnetoresistance for  $\text{La}_{5/6}\text{Li}_{1/6}\text{MnO}_3$ ,  $\text{La}_{2/3}\text{Bi}_{1/6}\text{Li}_{1/6}\text{MnO}_3$ ,  $\text{La}_{3/4}\text{Li}_{1/4}\text{MnO}_3$  and  $\text{La}_{1/2}\text{Bi}_{1/4}\text{Li}_{1/4}\text{MnO}_3$  samples at  $H = 10$  and  $50$  kOe



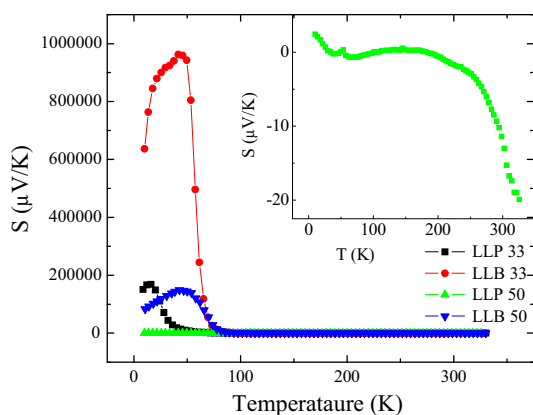


**Fig. 5** Variation of thermopower with temperature (10–325 K) of  $\text{La}_{5/6}\text{Li}_{1/6}\text{MnO}_3$ ,  $\text{La}_{2/3}\text{Bi}_{1/6}\text{Li}_{1/6}\text{MnO}_3$ ,  $\text{La}_{3/4}\text{Li}_{1/4}\text{MnO}_3$  and  $\text{La}_{1/2}\text{Bi}_{1/4}\text{Li}_{1/4}\text{MnO}_3$  samples. Inset of figure shows the  $S(T)$  behavior for  $\text{La}_{3/4}\text{Li}_{1/4}\text{MnO}_3$  sample

temperature and exhibits maximum in the low-temperature region. The observed behavior for these samples may be understood in the scenario of spin tunneling across the grain boundaries.

The Seebeck coefficient ( $S$ ) is defined as  $\Delta V/\Delta T$ , the thermoelectric voltage per degree of temperature difference. The Seebeck coefficient measured as a function of temperature,  $S(T)$  for all the samples is shown in Fig. 5. Over the measured temperature range, the sign of  $S$  values is positive for LLP 33 and LLB 33 samples indicating p-type conduction and the majority charge carriers are holes in these samples. Moreover, the sign of  $S$  changes from positive to negative at  $T = 37$  and  $228$  K for LLP 50 and LLB 50 compounds, respectively, thereby signifying electron- to hole-like conduction. In fact, similar behavior was reported by Mahendran et al. [37] in the case of LCMO and LSMO compounds and found that  $S$  becomes more negative with increase in  $\text{Mn}^{4+}$  content. It can be noticed from the figure that except for LLP 50, the thermal variation of thermopower is similar for all the samples; i.e.,  $S$  increases slowly with decreasing temperature and at a particular temperature  $T_{\text{max}}$  thermopower reaches maximum value and decreases thereafter. On the other hand, in the case of LLP 50,  $S$  increases with decreasing temperature initially and varies slowly on further lowering of temperature exhibiting a broad hump (inset of Fig. 5). In comparison with the parent compound (LLP 33 and LLP 50), the magnitude of  $S$  increases with Bi doping, and it may be noted from the figure that LLB 33 sample exhibits colossal thermopower in the low-temperature region. To the best of our knowledge, this is the largest value reported for manganites. Such an increase in  $S$  values at low temperatures was also reported in other manganites [38]. It has been found [39] that several factors such as impurity, complicated band structure, electron–phonon, electron–

magnon scattering affect the  $S(T)$  behavior. Hassen and Mandal [40] reported a large value of  $S$  in the case of  $\text{Sm}_{0.5}\text{Sr}_{0.5}\text{MnO}_3$  manganite and attributed to the charge-ordered phase transition. These results clearly suggest the contributions from electronic instabilities such as Jahn–Teller distortion, charge-/orbital-ordering, AFM interactions become important in explaining the thermopower behavior. From the temperature- and field-dependent magnetization (Fig. 2) results, it is clear that an inhomogeneous state exists in the low-temperature region. The competition between these two different phases leads to the enhancement of spin scattering which in turn may be responsible for the exhibition of large thermopower values.

### 3.4 Conduction mechanism

The formation of small lattice polarons in manganites due to strong electron–phonon interaction is a well-known phenomenon. In the case of adiabatic small polaron hopping (SPH), the transport is governed by the thermally activated hopping of charge carriers. According to the SPH model [41], the expression for resistivity is given by,

$$\rho(T) = \rho_\alpha T \exp(E_p/k_B T)$$

where  $E_p$  is the activation energy and  $\rho_\alpha = 2k_B/3ne^2a^2v$ ; here  $k_B$  is Boltzmann’s constant,  $e$  is the electronic charge,  $a$  is site-to-site hopping distance, and  $v$  is the longitudinal optical phonon frequency. From the slopes of  $\ln(\rho/T)$  versus  $(1/T)$  plots (Fig. 6), the activation energy ( $E_p$ ) values were estimated and are given in Table 2. A linear relation in the figure shows that the electrical transport behavior can be described with a small polaron hopping model. Recently, a number of reports suggest that polaron effects contribute to transport mechanism of manganites in both insulating and metallic states. This allows the consistent interpretation of resistivity in the whole temperature and phase range [42, 43].

The thermopower data in the high-temperature regime ( $T > T_C$ ) is well described by a polaronic phase with a  $T^{-1}$  dependence according to the following equation [41],

$$S = k_B/e[E_S/k_B T + \alpha']$$

where  $E_S$  is the activation energy obtained from TEP data.  $\alpha'$  is a constant of proportionality between the heat transfer and the kinetic energy of an electron, and it can be used to ascertain the type of polarons that are participating in conduction process.  $\alpha' < 1$  suggests the conduction is due to small polarons and  $\alpha' > 2$  suggests the existence of large polarons. Figure 6 shows the  $S$  versus  $1/T$  curve for LLP 50 and LLB 50 samples, and the solid lines give the best fit to the above equation. The values of activation energy  $E_S$  and  $\alpha'$  were obtained from the best fit and are given in Table 2. It is clear from the table that  $E_p$  and  $E_S$  values are found to

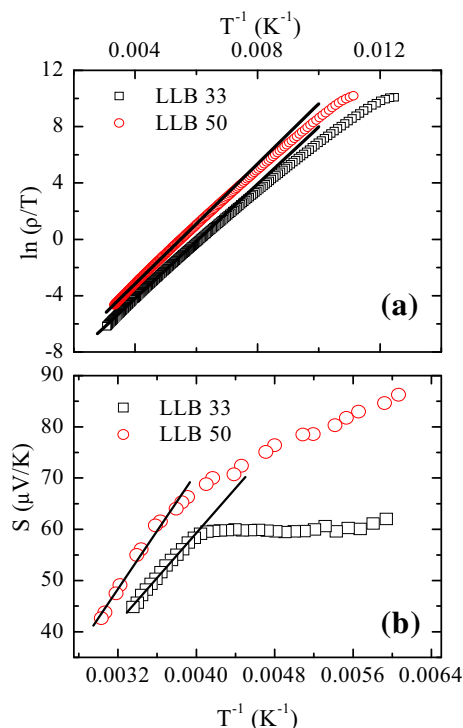


**Fig. 6** **a** Plots of  $\ln(\rho/T)$  versus  $T^{-1}$  for  $\text{La}_{2/3}\text{Bi}_{1/6}\text{Li}_{1/6}\text{MnO}_3$  and  $\text{La}_{1/2}\text{Bi}_{1/4}\text{Li}_{1/4}\text{MnO}_3$  samples. The *solid line* shows the best fit of data with an equation  $\rho(T) = \rho_2 T \exp(E_p/k_B T)$ . **b**  $S$  versus  $T^{-1}$  behavior for the samples,  $\text{La}_{2/3}\text{Bi}_{1/6}\text{Li}_{1/6}\text{MnO}_3$  (*open black square*) and  $\text{La}_{1/2}\text{Bi}_{1/4}\text{Li}_{1/4}\text{MnO}_3$  (*open red circles*), and *solid lines* are the best fits to SPH model at high temperature

increase with Bi doping and this may be attributed to the special electronic structure of  $\text{Bi}^{3+}$  ion and its distribution in  $\text{LaLiMnO}_3$ . With the Bi doping, a larger distortion state might occur in the perovskite structure leading to the formation of pinning center, thereby resulting in the increase of activation energy. It is clear from the table that the magnitudes of  $E_p$  are higher than  $E_s$  values in the samples. In the framework of small polaron conduction model,  $E_p$  is the sum of the activation energy required for the creation of the carriers and activating the carriers for hopping while  $E_s$  is the energy required to activate the carriers for hopping. In view of this,  $E_p$  is always higher than  $E_s$ . Additionally, the obtained values of  $\alpha' < 1$  in these manganites manifest that the conduction in the present system is due to small polarons.

#### 4 Conclusions

The effect of bismuth doping on magnetic and transport properties of lanthanum lithium manganites having fixed  $\text{Mn}^{3+}/\text{Mn}^{4+}$  ratio has been investigated systematically. The  $\rho(T)$  exhibits an insulating behavior, and

ferromagnetic to paramagnetic transition decreases upon Bi doping. The results were attributed to the lone-pair effect due to Bi doping. The LLP 50 samples show typical feature of intergrain and intrinsic MR in the low-temperature region and near  $T_p$  (300 K). Among the samples of the present investigation, LLB 33 compound exhibits colossal thermopower (0.9 V/K) in the low-temperature region which may be exploited for thermoelectric applications. Finally, the resistivity and thermopower data in the high-temperature region are explained within the framework of small polaron hopping mechanism.

**Acknowledgments** The first author (YKL) is grateful to CSIR for providing fellowship. The authors also acknowledge DST, Govt. of India, for funding 14T PPMS. The authors also thank Centre Director, Dr. A. Banerjee and Dr. G. S. Okram of UGC-DAE CSR, Indore, India, for providing magnetization and thermopower facilities. The authors are grateful to Dr. J. Arunachalam, Director and A. C. Sahayam, CCCM, Hyderabad, for ICP-AES measurements.

#### References

1. J.B. Goodenough, *Phys. Rev.* **100**, 564 (1955)
2. Y. Tokura, N. Nagaosa, *Science* **288**, 462 (2000)
3. E. Dogotto, T. Hotta, A. Moreo, *Phys. Rep.* **344**, 1 (2001)
4. M.D. Coey, M. Viret, S. von Molnar, *Adv. Phys.* **48**, 167 (1999)
5. Z. Jirak, F. Damay, M. Hervieu, C. Martin, B. Raveau, G. Andre, F. Bouree, *Phys. Rev. B* **61**, 1181 (2000)
6. H.Y. Hwang, S.-W. Cheong, P.G. Radaelli, M. Marezio, B. Batlogg, *Phys. Rev. Lett.* **75**, 914 (1995)
7. N. Abdelmoula, E. Dhahri, K. Guidara, J.C. Joubert, *Phase Transit.* **69**, 215 (1999)
8. L.M. Rodriguez-Martinez, J.P. Attfield, *Phys. Rev. B* **54**(15), 622 (1996)
9. J. Topfer, J.B. Goodenough, *J. Solid State Chem.* **130**, 117 (1997)
10. J.M. Gonzalez-Calbet, E. Herrero, N. Rangavittal, J.M. Alonso, J.L. Martinez, M. Vallet-Regi, *J. Solid State Chem.* **148**, 158 (1999)
11. N. Abdelmoula, K. Guidara, A. Cheikhrouhou, E. Dhahri, J.C. Joubert, *J. Solid State Chem.* **151**, 139 (2000)
12. S.-W. Cheong, H.Y. Hwang, in *Condensed Matter Science, Ch. 7*, ed. by Y. Tokura (Gordon and Breach, Reading, 2000)
13. A. Moreo, S. Yunoki, E. Dagotto, *Mater. Sci.* **283**, 2034 (1999)
14. N.D. Mathur, P.B. Littlewood, *Solid State Commun.* **119**, 271 (2001)
15. C. Zener, *Phys. Rev.* **81**, 440 (1951)
16. A.J. Millis, P.B. Littlewood, B.I. Shraiman, *Phys. Rev. Lett.* **74**, 5144 (1995)
17. X.L. Wang, S.J. Kennedy, P. Gehringer, W. Lang, H.K. Liu, S.X. Dou, *J. Appl. Phys.* **83**, 7177 (1998)
18. S.L. Ye, W.H. Song, J.M. Dai, S.G. Wang, K.Y. Wang, C.L. Yuan, Y.P. Sun, *J. Appl. Phys.* **88**, 5915 (2000)
19. T. Shimura, T. Hayashi, Y. Inaguma, M. Ioth, *J. Solid State Chem.* **124**, 250 (1996)
20. Y. Kalyana Lakshmi, G. Venkataiah, P. VenugopalReddy, *J. Appl. Phys.* **106**, 023707 (2009)
21. J.H. Hao, Z.S. Li, H.K. Wong, *Mater. Sci. Eng., B* **83**, 70 (2001)
22. J. Wu, S.-Y. Zhang, *J. Magn. Magn. Mater.* **264**, 102 (2003)
23. N. Ghosh, Suja Elizabeth, H.L. Bhat, U.K. Robler, K. Nenkov, S. Robler, K. Dorr, K.-H. Muller, *Phys. Rev. B* **70**, 184436 (2004)

24. Z.C. Xia, L.X. Xiao, C.H. Fang, G. Liu, B. Dong, D.W. Liu, L. Chen, L. Liu, S. Liu, D. Doyananda, C.Q. Tang, S.L. Yuan, J. Magn. Magnet. Mater. **297**, 1 (2006)
25. Z.C. Xia, G. Liu, B. Dong, L. Chen, D.W. Liu, C.H. Fang, D. Doyananda, L. Liu, S. Liu, C.Q. Tang, S.L. Yuan, J. Magn. Magnet. Mater. **292**, 260 (2005)
26. R. Li, Z. Qu, J. Fang, Phys. B **406**, 1312 (2011)
27. A. Soni, G.S. Okram, Rev. Sci. Instrum. **79**, 125103 (2008)
28. Z.C. Xia, Y. Wang, H.R. Zeng, Q.X. Zhou, M.T. Hu, B. Dong, G. Liu, X.N. Feng, L. Liu, S.L. Yuan, C.Q. Tang, Solid State Commun. **137**, 216 (2006)
29. J.L. Garcia-Munoz, C. Frontera, M.A.G. Aranda, A. Llobet, C. Ritter, Phys. Rev. B **63**, 064415 (2001)
30. B.H. Kim, J.S. Kim, T.H. Park, D.S. Lee, K.H. Kim, B.G. Kim, Y.W. Park, J. Phys.: Condens. Matter **19**, 296205 (2007)
31. J.M.D. Teresa, M.R.P. Ibarra, A. Algarabel, C. Ritter, C. Marquina, J. Blasco, J. Garcia, A.D. Moral, Z. Arnold, Nature **386**, 256 (1997)
32. M. Mayr, A. Moreo, J.A. Verges, J. Arispe, A. Feiguin, E. Dogotto, Phys. Rev. Lett. **86**, 135 (2001)
33. R. Li, Z. Qu, J. Fang, Phys. B **406**, 1312 (2011)
34. N.A. Hill, K.M. Rabe, Phys. Rev. B **59**, 8759 (1999)
35. L.W. Lei, Z.Y. Fu, J.Y. Zhang, Mater. Lett. **60**, 970 (2006)
36. H.Y. Hwang, S.W. Cheong, N.P. Ong, B. Batlogg, Phys. Rev. Lett. **77**, 2041 (1996)
37. R. Mahendiran, S.K. Tiwary, A.K. Roychaudhuri, T.V. Ramakrishnan, R. Mahesh, N. Rangavittal, C.N.R. Rao, Phys. Rev. B **53**, 3348 (1996)
38. S. Taran, B.K. Chaudhuri, S. Chatterjee, H.D. Yang, S. Neelshwar, Y.Y. Chen, J. Appl. Phys. **98**, 103903 (2005)
39. P. Mandal, Phys. Rev. B **61**, 14675 (2000)
40. A. Hassen, P. Mandal, J. Appl. Phys. **101**, 113917 (2007)
41. N.F. Mott, E.A. Davis, *Electronics Process in Non Crystalline Materials* (Clarendon, Oxford, 1971)
42. J. Hoffmann, P. Moschkau, S. Mildner, J. Norpoth, Ch. Jooss, L. Wu, Y. Zhu, Mater. Res. Express **1**, 046403 (2014)
43. P. Graziosi, A. Gambardella, M. Prezioso, A. Riminucci, I. Bergenti, N. Homonnay, G. Schmidt, D. Pullini, D. Busquets-Mataix, Phys. Rev. B **89**, 214411 (2014)